Investigation Of The Residual Capacity Of Built-Up Columns With Different Configurations And Web Stiffeners Under Post-Fire Conditions

Wenjie Li*

Shanxi Vocational University of Culture and Tourism, Taiyuan 030000, China

*Corresponding author. E-mail: liwenjie198206@163.com

Received: Oct. 13, 2025; Accepted: Apr. 27, 2026

In structural applications, CFS (cold-formed steel) built-up columns with web stiffeners are widely used for their lightweight and high load-carrying capacity. However, this study examines CFS-built-up columns under post-fire axial compression using validated ABAQUS models. Configuration B shows up to 22.4% higher load capacity than Configuration A between 700°C and 900°C. CS- and CU-shaped columns are stronger among the various stiffener geometries considered, while C-shaped columns are the least effective in resisting loads. Additionally, the use of wider stiffeners ($b/4 = 12.75$ mm) outperforms narrower ones ($b/6 = 8.5$ mm) by up to 15% at high temperatures, and longer stiffeners (b) provide a 14% increase in load capacity compared to shorter stiffeners (b/3). These findings validate that an optimized stiffener design improves structural efficiency and fire resistance. Hence, these findings have important implications for the design of fire-resistant CFS structures.

Keywords: CFS; post-fire; residual capacity; web stiffener; column configuration; numerical analysis; ABAQUS

http://dx.doi.org/10.6180/jase.202610_33.047

1. Introduction

Built-up steel columns are widely used because combining several steel members into a single column can increase resistance and stability under compression compared with individual members. Yet, their behavior is prone to the influence of production and assembly effects, as highlighted by the findings of Röß et al. [1] regarding the impact of innovative highstrength steel composite column sections. Web stiffeners are often used in steel members to delay buckling and increase stiffness. The findings from steel members and the behavior of the thin-walled sections implied the significant influence of stiffener size and layout on lateral and distortional instability modes, as reported by Bui et al. [2] and Shaat et al. [3], and the enhancement of the resistance against buckling of cold-formed steel column members, as discussed and reported by Palanivelu et al. [4]. In this regard, the numerical studies on mode interaction of web-stiffened members, as reported and conducted by Deepak and Aravinth [5], and the innovative closed built-up sections of cold-formed steel, as reported and conducted by Jiang et al. [6], showed the influence of geometric and stiffening parameters, along with the controlling mode of the section buckling. Steels exposed to fire and then cooled might experience microstructural alterations and degradation in their mechanical properties, which directly influence RRS and stability. The relationship between metallographic alteration and variation in mechanical properties after fire was established by Hua et al. [7], and the mechanical behavior of steels after fire was measured by experimental work conducted by Dan et al. [8]. In the case of high-strength steel, the mechanical properties of Q690 steel after fire were investigated by Li et al. [9] and Wang et al. [10] conducted experimental and numerical research on the behavior of Q960 steel columns after fire. At the member level, Xue et al. [11] suggested that the behavior after fire was governed by instability in cold-formed Q960 ultra-high-strength steel channel stub columns, and further evidence was provided by Lan et al. [12] on hot-rolled stainless steel channel stub columns exposed to fire. All these investigations have shown that material modeling is necessary and dependent on material grade and cooling conditions, and that material behavior should be evaluated with a focus on stability. In addition to coupon-scale characterization, several studies have evaluated residual performance at the member-system level in post-fire steel structures. Maraveas et al. [13] reviewed post-fire assessment and rehabilitation of steel structures, emphasizing the role of connection components (high-strength bolts) and residual deformations in evaluation results. Molkens et al. [14] assembled an extensive post-fire material data set and suggested retention coefficients with specified safety coefficients for uniform post-cooled numerical evaluation of structural carbon steel materials. Earlier, Franssen and Kodur [15] illustrated numerical procedures for computing residual load-carrying capacity in representative case studies after a fire event. Member-level evaluation of post-fire steel structure performance was attempted by Pantousa et al. [16], who proposed validated numerical simulations of post-fire steel columns, postulating that post-fire behavior depends on combined residual deformations, the specified thermal history, and an applied post-fire material model. Post-ISO-834 simulation data for high-strength steel columns were also augmented experimentally and numerically by Wang and Liu [17], underscoring the role of fire duration, cooling rate, and topological slenderness. In the specific field of CFS built-up columns, Yang et al. [18] illustrated how the detail of connections (such as the distance of the screws) represents a fundamental factor capable of controlling the behavior of the box-shaped built-up CFS column. Evidence has extended postfire analyses to these issues: Luo et al. [19] investigated back-to-back CFS built-up columns controlled by local buckling failures, providing post-fire expressions for predicting the residual capacity of SCI/CEN members through a combination of tests and validation calculations, subsequently extending the work for distortional-buckling-controlled scenarios involving the same configuration of structures exposed to elevated temperatures, with a particular emphasis on the role of distortional slenderness [20]. Zhang et al. [21] investigated the response of temperature-varyingly exposed CFS box-shaped built-up columns, providing information on the impact of pre-fire stiffening on post-fire residual resistance, together with new formulae for predictive modeling of CFS behavior based on post-fire reduction factors. Also, targeting mode characterization, another line of CEN-code class CFS post-fire structural analysis concerns the local and distortional buckling behavior of back-to-back channels in the specific case of postfire analysis of Al-alloy columns [22], providing additional benchmarks for best practices in post-fire computation of this structural behavior for comparison purposes. For design purposes, the post-fire scenario available today indicates the need to adjust the currently available CEN structural analysis for CFS members [10]; nevertheless, the available post-fire data indicate the need for specific post-fire adjustments to accurately compute residual capacity in these structural members.

There are still three areas for improvement. First, the post-fire analyses on CFS built-up columns are still limited to a few built-up configurations (mainly back-to-back or box-like) and simplified stiffening systems, and the current understanding of the combined effect of the configuration type (open or closed systems) and the web stiffener design on the post-fire stability problem remains insufficient [18–21]. Second, whereas post-fire material degradation and instability phenomena in high strength steels and CF steel members [9–11], among others, are known, a complete synthesis on the combined role of material degradation and instability, residual stresses [1], geometric imperfections, weakening due to connectors [15–17], and switching between modes/local-distortion interaction [4–6], over a broad parameter range, has never been attempted before. Third, whereas some enhanced schemes for post-fire predictions are proposed and explored in selected cases [19–21], general guidance within the shape space defined in a proper cold-formed framework [22] remains unavailable. This study addresses the three identified gaps and focuses on the development and validation of a finite element modelling framework on post-fire built-up steel columns with web stiffeners over a broad range of geometric configurations.

2. Materials and methods

2.1. Finite Element Modelling

2.1.1. General Overview

This work aims to predict the axial compressive post-fire loading behavior of a built-up section with precision using a nonlinear elastic-plastic finite element model (FEM) in ABAQUS (Figure 1a). FEM was initially validated against the corresponding empirical outcomes. The material property derived from the research conducted by Roy et al. [23] was integrated into parametric investigations. The modeling technique included elastic buckling analysis to derive eigenvectors, which were subsequently used to replicate the initial geometric imperfections.

2.1.2. Material Properties

The columns' relative lengths were established using a constitutive model that considered both elastic and plastic behavior. This material's isotropic yielding and plastic hardening characteristics were analyzed using the von Mises yield surface within a traditional metal plasticity framework. Using the given formulae, the ABAQUS user handbook transformed the engineering stress-strain curves into the appropriate ones:

$$\sigma_{\text{true}} = \sigma_{\text{nom}} \left(1 + \varepsilon_{\text{norm}}\right) \tag{1}$$

$$\varepsilon_{ln}^{pl} = \ln\left(1 + \varepsilon_{\text{nom}}\right) - \frac{\sigma_{\text{true}}}{E} \tag{2}$$

where σ_{true} and ε_{ln}^{pl} represent the genuine strain as well as stress, in that order, while σ and ε symbolize stress and strain in engineering.

2.1.3. Mesh Size and Element Type

The S4R shell finite element model in ABAQUS, composed of four-noded linear quadrilateral shell elements with six degrees of freedom per node, was employed to analyze back-to-back built-up column sections. In assessing the mesh independence of results derived from the selected mesh size, mesh sensitivity analysis was performed to ascertain if any biases exist against using a specific mesh. The built-up column sections were modeled in ABAQUS software using four-node linear quadrilateral shell elements called 'S4R' elements, having six degrees of freedom per node. Three different mesh sizes, namely 2 mm, 5 mm, and 10 mm, were used in the model as depicted in Figure 1b, and the comparison was done with the experimentally determined ultimate capacity. The study observed that the predicted ultimate load is not significantly affected by the mesh size. Thus, it was decided to deploy a 5 mm × 5 mm mesh, as it is a rational choice with an aspect ratio close to unity.

2.1.4. Contact and Boundary Conditions

The model's boundary constraints, such as pin-ended column configurations, were designed to mimic empirical processes. The column's peak served as the reference point, positioned midway down the final length. This reference point established the boundary conditions by employing a BEAM MPC to limit the rotational and translational degrees of freedom of the cross-section nodes with respect to this reference point (Fig. 1b). Every rotational and translational degree of freedom was constrained entirely by the reference point constraints, except the axial direction. An axial movement at the reference point applied a compressive force, mimicking a compression load on the column. The method above facilitates accurate load regulation and

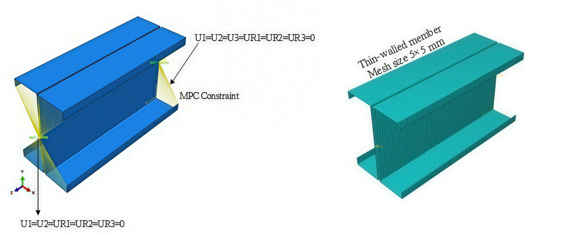

(a) FEM

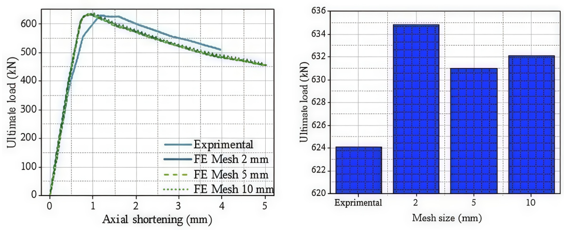

(b) Mesh sensitivity analysis

Fig. 1. Finite element modelling and mesh sensitivity analysis

boundary condition implementation, enhancing reliability and accuracy in finite element model simulations.

2.1.5. Geometric Imperfection

To account for initial geometric imperfections due to local and distortional buckling, an eigenvalue-based analysis was performed, and the mode shapes were used to define the initial imperfections in the subsequent analysis. In ABAQUS, an eigenvalue analysis was conducted on the built-up column, and the mode shape was identified as an integration of distortional buckling and local buckling of the web. This mode shape was used as the primary geometric imperfection in the analysis, consistent with earlier studies. The primary geometric imperfection was introduced by the first elastic buckling mode, having a magnitude of $t/10$, following previously validated numerical studies of similar cold-formed HSS and UHSS channel stub columns. The method was adopted to introduce a realistic imperfection profile into the analysis model [24, 25]. The model used a $t/10$ value to represent the defect size because t represents the plate thickness. Fig. 2 shows a sample mode shape of the stub column. As can be seen, the local instability of the web in the out-of-plane direction is already embedded in the selected eigenmode. Thus, in this simulation, local geometrical imperfection is considered using the use of local eigenmode imperfections. No residual stresses were considered directly in this work. The research team did not study membrane residual stress because its magnitude was lower than the bending residual stresses. Bending residual stresses were not considered directly since the material at-

Table 1. Comparison of time performance and performance with different superpixel methods

Specimen	P_{EXP} (kN)	P_{FE} (kN)	P_{EXP}/P_{FE}(kN)	Failure mode
BU240-S50-L300-1	121.28	118.9	1.02	LB + DB

Note: LB = Local buckling; DB = Distortional buckling.

tributes of the flat and corner parts are already determined based on the tensile test results [24, 25].

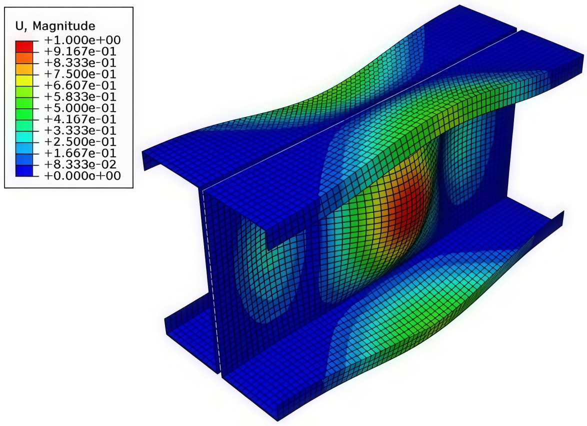

Fig. 2. First buckling mode of the stub column

2.2. Validation of the Numerical Model

The experiment compared empirical data from the test specimen, BU240-S50-L300, a built-up stub column, to confirm the accuracy and reliability of the developed FEM. This experiment serves as an evolutionary benchmark for comparative analyses. A comparison is made between quantitative and empirical data regarding load capacity, axial load vs axial shortening, and failure modes. Through the comparative study, FEM provides an accurate representation of the behavior of built-up columns constructed from CFS. The axial strength testing and BU240's FEA are shown in Table 1. Table 1 indicates that the strengths attained from finite element analysis (FEA) closely align with the empirical data. Fig. 3a shows the stub's load-versus-axial-shortening characteristics, along with short columns derived from finite-element analysis and testing data. Minimal disparity was observed between FEM predictions and empirical outcomes. The ratio of empirical to numerical outcomes (P_{EXP} / P_{FE}) has a coefficient of variation of 0.06 and a mean of 1.02. Fig. 3b illustrates the distorted stub and short-column layouts from the finite-element analysis, which closely align with the empirically observed failure modes.

To further demonstrate the practicability of this adopted numerical modeling framework for modeling steel members under post-fire conditions, additional validation will be conducted using independent experimental data from steel channel-section stub columns subjected to fire conditions. In this case, validation of this framework will be based on two cases, which include: fire-exposed hot-rolled stainless steel stub column specimens reported by Lan et al. [12] (specimen C2-1000); and post-fire cold-formed ultra-high-strength steel stub column specimens reported by Xue et al. [11] (specimens C3-S1 and 120 × 90). For both cases, specimens were subjected to prescribed fire exposure and subsequent cooling to ambient temperature before undergoing axial compression tests, so that this comparison relates to a post-fire structural analysis. For each

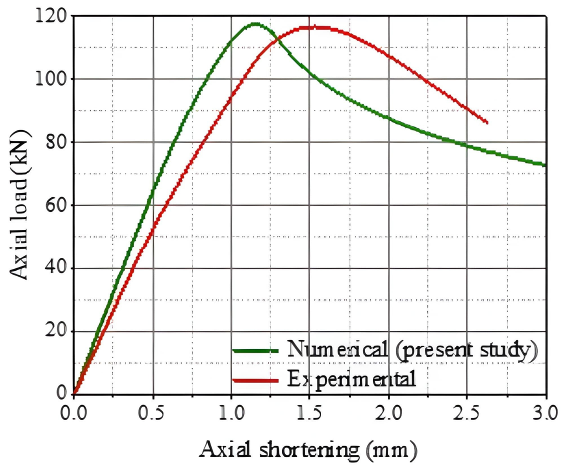

(a) Validation

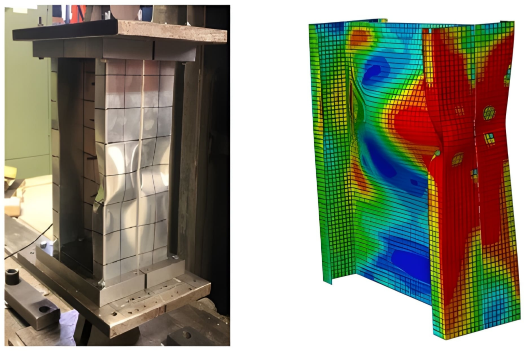

(b) Failure modes [23]

Fig. 3. Validation and failure mode comparison of the BU240-S50-L300 built-up stub column

chosen specimen, the numerical model was developed using the same modelling tactic as explained in the earlier segments (element formulation, boundary conditions, loading scheme, contact definition, if required, and geometric imperfections). The geometry of the specimens, as well as the test arrangement for each case, has been modelled according to the experimental setups reported in the literature, with the axial compression response simulated as load-displacement curves. For the post-fire properties of the materials, the relevant information from the experimental research for each case is used to align with the experimental conditions. In Fig. 4, the expected and test axial loaddisplacement curves are compared for specimen C2-1000 (Lan et al. [12]) and specimens C3S1 and 120 × 90 (Xue et al. [11]). Table 2, a comparison between the peak load predicted by finite elements and test results is summarized for the post-fire steel stub columns chosen. A juxtaposition between the expected and test results is carried out using a ratio and an error percentage relative to the test results.

Another verification was performed on a built-up steel column with a stiffener. Validation was performed by comparing the numerical results with the experimental data of Hady et al. [26] for built-up cold-formed steel columns. Specimens 45A90C112 and 60A60C150 were chosen as reference cases. FEM is displayed in Fig. 5, while Table 3 presents the empirical outcomes compared with the numerical predictions. As for the experimental analysis, specimen 45A90C112 exhibited an ultimate load of 237.32 kN and failed by local-flexural buckling, while specimen 60A60C150 reached 418.20 kN and failed by local-flexural-distortional buckling. Conversely, based on FEM, ultimate loads of 277.30 kN and 454.40 kN are obtained, representing errors of 16.85% and 8.66%, respectively. Load-displacement behavior was found to be highly accurate in the elastic and early stages of inelastic range (see Figure 6); however, some differences were observed in the post-buckling stage, which may be attributed to initial material and geometrical imperfections.

2.3. Parametric Study

The axial compression performance of built-up CFS columns after fire was thoroughly analyzed using parametric studies. The main purpose of this research project involves determining how much strength remains in columns, and their deformation after they have experienced extreme fire heat. Seventy-eight numerical models were created and examined with the finite element program Abaqus. The post-fire material characteristics of high-strength Q690 steel were obtained from the empirical research conducted by Li et al. [9]. Li et al. [9] have presented

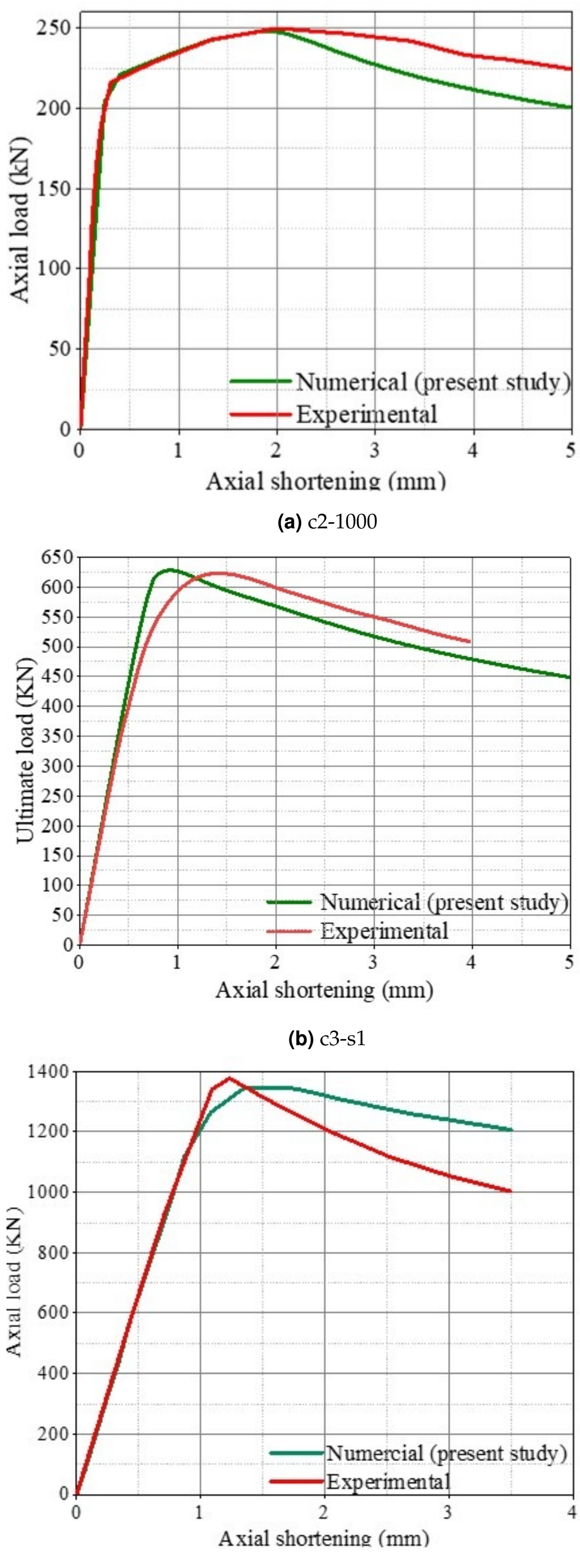

(a) c2-1000

(b) c3-s1

(c) 120*90 [11, 12]

Fig. 4. Juxtaposition between empirical and numerical outcomes of specimens

Table 2. Comparison of experimental and FE peak axial loads for post-fire steel stub columns [11, 12]

Specimen	P_{EXP} (kN)	P_{FE} (kN)	$\boldsymbol{P_{FE}/P_{EXP}}$	Error (%) [a]
C3-S1	625.60	631.00	1.009	+0.86
120 × 90	1347.76	1377.53	1.022	+2.21
C2-1000	249.77	248.23	0.994	-0.62

[a] Error (%) $= (P_{FE} - P_{EXP}) / P_{EXP} \times 100$

Table 3. Comparison of experimental and FE Results

Specimen	Experimental Load (kN) [26]	Numerical Load (kN)	Exp.% Difference
45A90C112	237.32	277.3	16
60A60C150	418.20	454.4	8.6

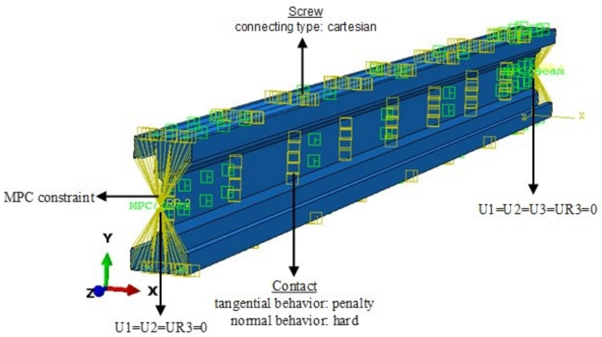

Fig. 5. Details of boundary conditions, screw arrangement, and contact interaction in the finite element model

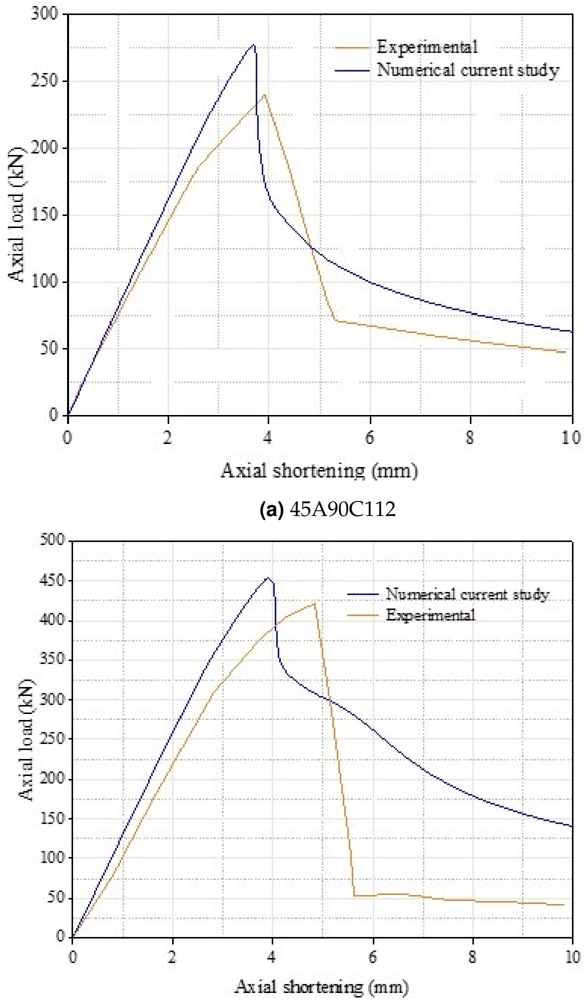

(a) 45A90C112

(b) 60A60C150

Fig. 6. Validation of the Numerical Model: (a) Specimen 45A90C112, (b) Specimen 60A60C150 [26]

a series of post-fire reduction factors for Q690 Steel that was exposed to high temperature and then allowed to cool. Specifically, the authors have provided reduction factors for the yield strength ratio ($f_{y,T}/f_y$), ultimate strength ratio ($f_{u,T}/f_u$), and elastic modulus ratio (E_T/E), as well as the various post-fire stress-strain curves that correspond to the maximum temperature exposure. In the current study, the posted fire-reduction factors and stress-strain curves from Li et al. [9] are used as representative of Q690 Steel's properties following exposure to and cooling from a fire event. The post-fire reduction factors and post-fire stressstrain curves taken from Li et al. [9] are included in Table 4 and Figs. 7a and 7b. The post-fire material model in ABAQUS was developed using a reduced elastic modulus and a multilinear plastic constitutive relationship derived from the stress-strain curve corresponding to the maximum temperature exposure in the current analysis. The research aims to evaluate how columns lose stiffness when exposed to fire, their resulting failure patterns, and their behavior under load displacement tests. Numerical model Type A and Type B configurations involved variations in the number of CFS components that made up the built-up section.

Table 4. Reduction factors for the post-fire mechanical attributes of Q690 structural steel

Temperature (°C)	$(f_{y,T}/f_y)$	$(f_{u,T}/f_u)$	(E_T/E)	$(\varepsilon_T/\varepsilon)$
20	1.00	1.00	1.00	1.00
300	1.08	1.02	1.00	0.91
500	0.98	0.94	1.00	1.03
700	0.64	0.67	1.01	1.86
900	0.46	0.60	0.99	2.43

Cross-sectional members were subsequently categorized into four groups based on the presence and configuration of web stiffeners: C-shaped without web stiffeners (C), C-shaped with V-shaped web stiffeners (CV), C-shaped with U-shaped web stiffeners (CU), and C-shaped with trapezoidal web stiffeners (CS). This classification enabled systematic examination of how different stiffening configurations and section geometries affected the columns' post-fire residual axial strength. The geometrical configurations of the columns corresponded to a distinct increase in the cross-sectional forms, as illustrated in Fig. 8. A coordinated nomenclature method was implemented to ensure consistent and precise identification of the specimens. Each model designation comprises four components arranged in the following sequence: the section type (C, CV, CU, or CS), the built-up configuration type (A or B), the stiffener width (a) relative to the flange width b(b/4 or b/6), and the web stiffener length (b) expressed as b/2, b/3, b, or 2 b/3. The designation CV-A-b/4-b/3 refers to a C-section using Vshaped stiffeners of configuration type A in built-up construction, with a stiffener width of a $=$ b/4 and a stiffener length of $\mathrm{b}_1 = \mathrm{b}/3$. The model's name is directly linked to the column's geometric and stiffening characteristics under the aforementioned naming system. The flange width (b_1) consistently measures 51 mm across all specimens, although the web stiffeners (a) width was designated as $b/4$ or $b/6$. The parameter b_1 was subsequently defined as $b/2, b/3, b$, or 2 b/3. They conducted these parametric changes to assess the impact of various geometric ratios on local, distortional, and global buckling responses after a fire event. Axial compression loading was applied to all numerical models to document the post-combustion loaddisplacement responses and evaluate residual strength, stiffness deterioration, and failure mechanisms. This work provides a comprehensive analysis of the behavior of built-up CFS columns in post-fire condition, accounting for the effects of geometry, stiffener configuration, and post-fire material deterioration. The findings are advantageous for optimizing design parameters and improving the safety and performance of built-up cold-formed steel structural systems in fire-damaged scenarios.

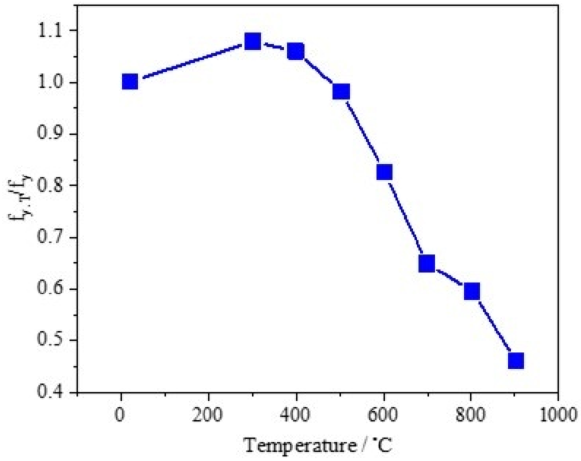

(a)

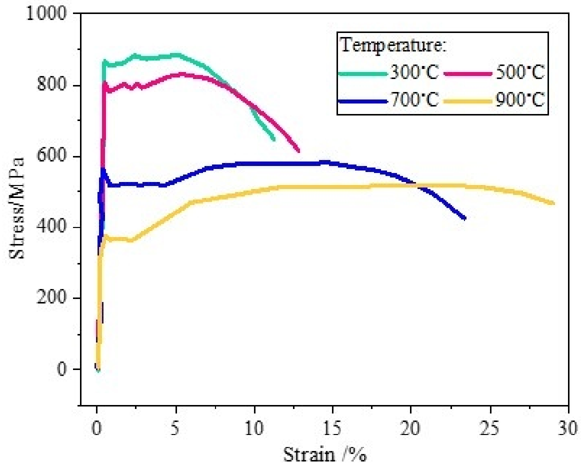

(b)

Fig. 7. (a) Post-fire yield-strength reduction factors for Q690 structural steel, (b) Post-fire stress-strain relationships for Q690 structural steel after exposure to various peak temperatures

3. Results and discussion

This exploration underscores the distinct structural response of the columns in terms of ultimate load-carrying capacity. The post-fire axial response is presented in load-axial displacement curves, which summarize the results of the different numerical models. Figs. 9a to 9c illustrate the numerical predictions in selected cases for configurations C, CV, CU, and CS to demonstrate the influence of key variables.

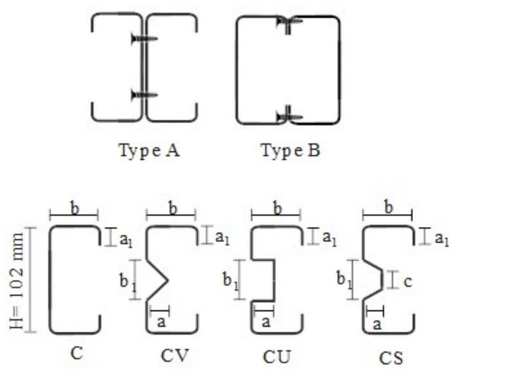

Cross-sectional member	b (mm)	a (mm)	a_1 (mm)	b_1 (mm)
C	51	12.5	-	-
CV, CU, CS	51	12.5	8.5	17,34
			12.75	25.5,51

Fig. 8. Built-up CFS column configurations and the cross-sectional members used in them contain webstiffener geometry

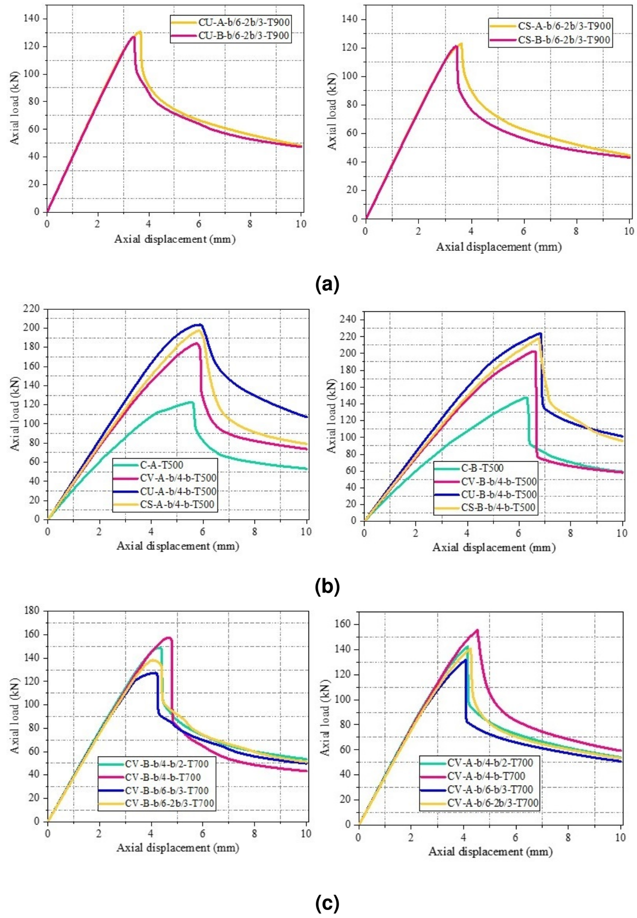

Fig. 9. Numerical simulations of several cases illustrating the effect of (a) column configuration, (b) stiffener shape, and (c) stiffener dimensions on the ultimate load-bearing capacity of the column

3.1. Effect of Column Configuration

High temperature analysis demonstrates how column design elements determine their ability to maintain strength after fire damage. Configuration B maintains a superior loadcarrying capacity than Configuration A at all temperatures. The difference between their performances grows larger as the temperature increases. For instance, at 20 °C, Configuration B has 8.1% better load-carrying ability compared to Configuration A. The superior behavior of Configuration B under normal conditions is maintained for higher temperatures. Configuration B is able to maintain better load-carrying capacity as seen in 700 °C and 900 °C temperatures, where it maintains 84.0% and 75.1%, respectively, whereas Configuration A only maintains 72.2% and 65.1%. This superior performance is due to effective load transfer and enhanced resistance to buckling failure. The reason behind the increased load capacity of Configuration B, despite high temperatures, which result in reduced material properties due to heating, can be explained through the effective interaction of components within the configuration. The strong interaction between stiffener members and columns in Configuration B delays buckling failure, leading to better post-fire performance (see Fig. 10a).

3.2. Effect of Column Stiffener Shape

The effects of stiffener shapes under different temperatures have been illustrated in Fig. 10b for Configurations A and B. The shape of the stiffener plays a vital role in the post-fire behavior of the column. Under ambient conditions, Configuration B with CS-stiffeners had the greatest strength compared to all other configurations, with a maximum of 8% increase compared to that of the C-shaped column without stiffeners. It should be noted that the effect of stiffeners becomes much more apparent under high temperatures. Specifically, when subjected to 500 °C heat, Configuration B, having CS stiffeners, was able to retain 95.5% of its load-bearing capacity, while the C-shaped unstiffened columns lost as much as 84.6% of their capacity. CS stiffeners enhance stability because they provide better protection against local buckling, which occurs near the web area. Thus, creating a more uniform stress pattern throughout the column length. As the temperature rises further, i.e.,

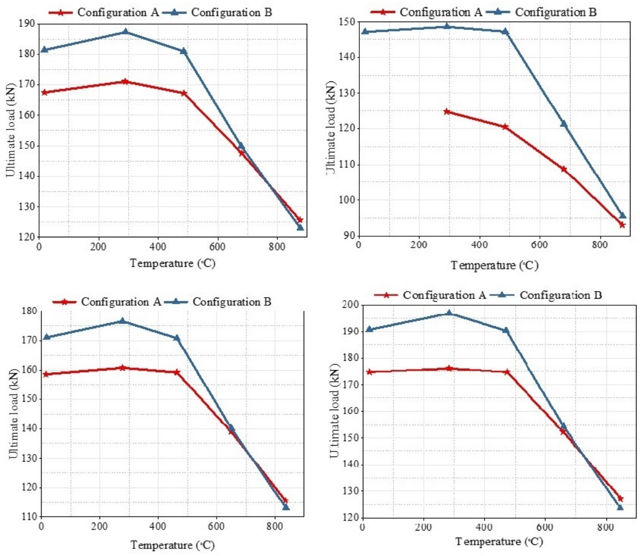

(a) effect of configuration

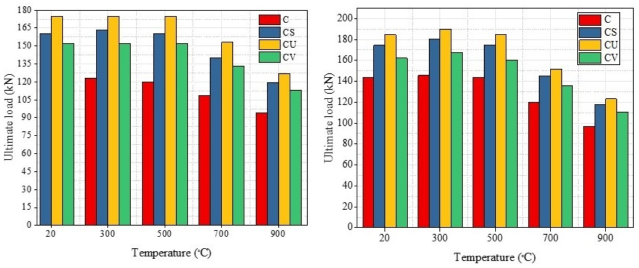

(b) effect of stiffener shape

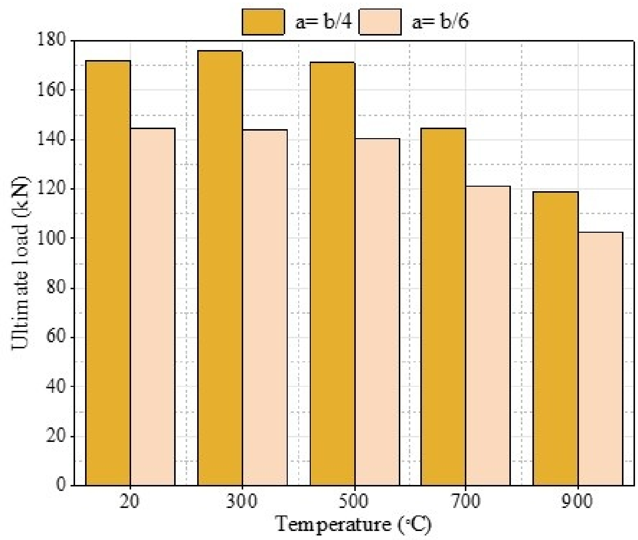

(c) effect of stiffener width (a =b/4 and a =b/6)

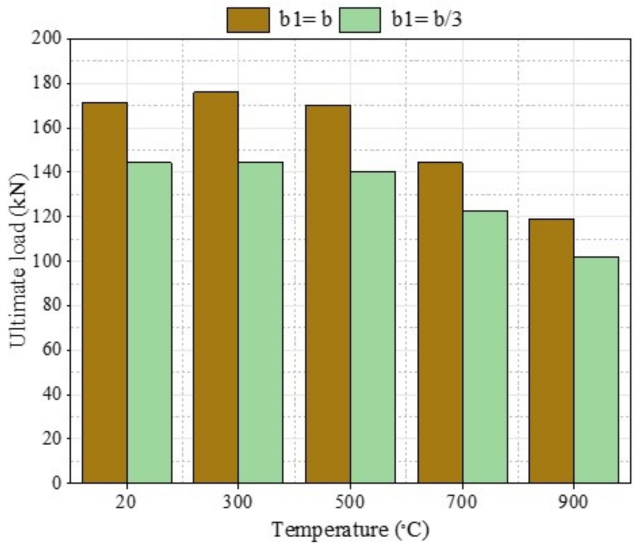

(d) effect of stiffener length (b1 =b and b1 =b/3)

Fig. 10. Ultimate load capacity in post-fire condition

700 °C and 900 °C, columns with V- and U-shaped stiffeners showed greater capacity to retain their loads due to greater resistance to distortional buckling.

3.2.1. Effect of Stiffener Width (a)

Fig. 10c illustrates the effect of stiffener width ($a = b/4$ and $a = b/6$) on ultimate load capacity under different temperature regimes. At 20 °C, columns with a stiffener width a = b/4 (12.75 mm) have greater ultimate load-carrying capacity than those with a stiffener width a = b/6 (8.5 mm). Fire resistance of columns depends on how wide the stiffeners are, which determine their ability to withstand structural loads. At 20 °C, columns with wider stiffeners (a = b/4) exhibited an 8.5% increase in load capacity compared to those with narrower stiffeners (a = b/6). This improvement can be attributed to the enhanced resistance to local buckling provided by the wider stiffeners. The stiffness of the column is directly linked to the width of the stiffeners, as wider stiffeners more effectively distribute axial loads and resist the onset of local instability under compressive forces. At higher temperatures, the difference between the two stiffener widths grew more significant. At 900 °C, columns with wider stiffeners retained 72.3% of their original strength, while those with narrower stiffeners only retained 65.1%. This trend highlights the superior thermal resistance of wider stiffeners, which mitigate the adverse effects of material degradation and promote greater load redistribution under fire-induced weakening. The column achieves better post-fire resistance because wider stiffeners maintain their stability when exposed to elevated temperatures.

3.2.2. *Effect of Stiffener Length (b1)*

Fig. 10d shows how stiffener length (b, $b/2$, $b/3$, $2b/3$) affects the ultimate load-carrying capacity of the column at different temperatures. The effect of stiffener length was also noted in the axial post-fire strength of the columns. In terms of ambient temperature, stiffened columns having larger stiffeners (b = b) showed the highest ultimate load carrying capacity, which is 15% higher than the stiffened columns having smaller stiffeners ($b = b/3$). Longer stiffeners are capable of redistributing the stress better along the length of the column, thereby avoiding buckling problems and improving the overall stiffness of the structure. Regarding high temperature, the benefits of using large stiffeners were also evident. At 700 °C, stiffened columns with larger stiffeners have only lost 13.1% of their strength compared to those stiffened columns with smaller stiffeners, which have already lost 21.5% of their strength. The same is true at 900 °C, where stiffened columns with longer stiffeners still have retained 26.4% of their strength compared to stiffened columns with smaller stiffeners that have only retained 35.9% of their strength.

3.3. Discussion on Failure Mode

The failure modes shown in the numerical analysis are a result of both local and distortional buckling. In configuration A, and especially the unstiffened C-profiles, there is premature local buckling of the web and flange areas after the attainment of maximum load capacity, specifically where failure is caused by fire damage. In configuration B, and especially where stiffeners CS and CU are used, there is a more stable pattern of failure. Premature local buckling of the web is avoided, with distortional buckling occurring in a controlled manner, thus showing better interaction between elements. The interaction between the stiffeners and the column sections will influence the failure modes as well. The use of wide and long stiffeners (b = b) leads to better load distribution, thus reducing local failures even under high temperature conditions. It is important to recognize the impact of stiffener design on the failure modes, as seen in this case, where wide and long stiffeners will cause a more stable failure mode that occurs due to controlled distortional buckling and not localized buckling. Figures 11a-c display that the failure modes caused by both local and distortional buckling after fire damage to the CFS columns become apparent. In this case, configuration B is better if the CS- and CU-type stiffeners have adequate width and length to resist local buckling but control distortional buckling.

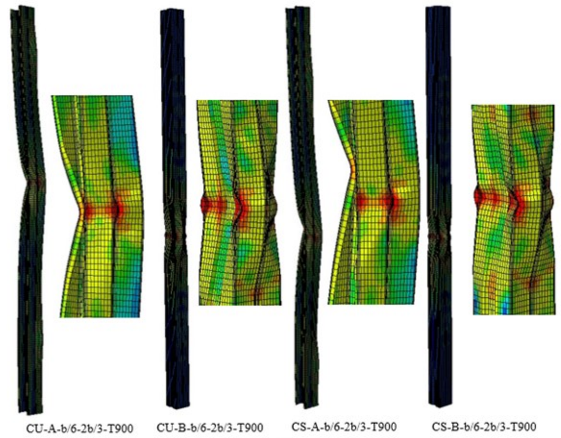

(a) column configuration

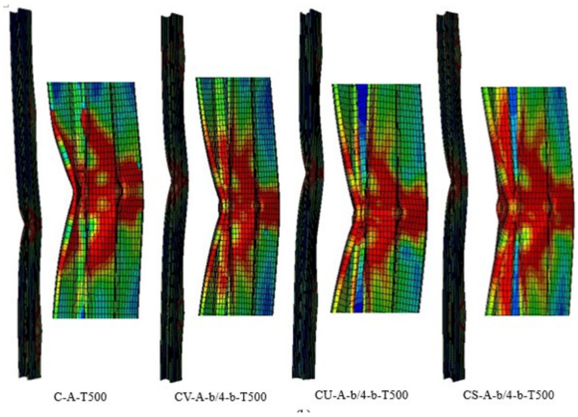

(b) stiffener shape

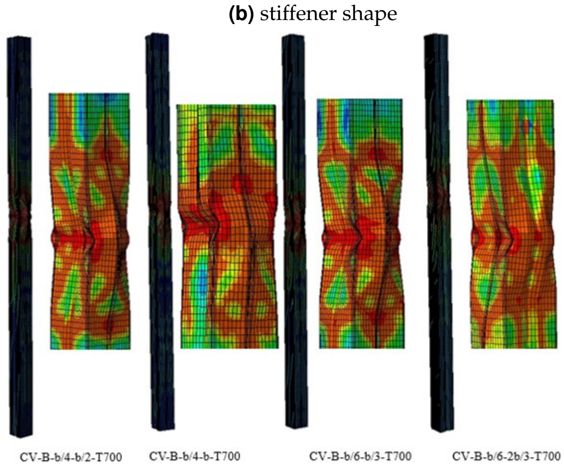

(c) stiffener dimension

Fig. 11. Effect of variables on failure modes of column

4. Conclusion

This study numerically investigated the post-fire axial compression behavior of coldformed steel built-up columns with different configurations and web stiffener parameters using validated ABAQUS models. Based on the parametric results, the following concise conclusions are drawn.

1. The arrangement of the built-up column affects its residual axial strength. It was found that the residual strength of Configuration B is higher compared to Configuration A throughout the range of studies conducted. This trend further highlights the importance of the structure of the built-up column on the effectiveness of force transmission after heat exposure.

2. The configuration of the web stiffener plays an important role in the performance after fire loading. In all the cases analyzed here, the columns with CS-shaped and CU-shaped stiffeners are stronger and behave more stably than those without any stiffeners with a similar profile to a "C.".

3. Increasing the stiffener width improved the residual performance of the columns. Columns with wider stiffeners generally maintained higher post-fire axial capacity than those with narrower stiffeners, indicating that wider stiffeners can enhance web stability and delay the development of local buckling after material degradation caused by fire.

4. Stiffener length was also found to affect post-fire behavior. Longer stiffeners generally provided higher residual strength than shorter ones, which may be attributed to improved stress redistribution and better restraint against local deformation in the web region.

5. The numerical investigation reveals the occurrence of failures wherein post-failure behavior is mainly dictated by the interplay of local buckling and distortional buckling. The degree to which these modes dominate is determined by the shape of the columns and their stiffener shapes. In general, stiffened sections are associated with late local buckling and better post-buckling performance.

5. Conflicts of interest

The author affirms that there are no conflicts of interest to disclose.

References

[1] R. Röß, M. Schäfers, and M. Mensinger. "Influence of residual stresses on innovative composite column sections using high strength steel". In: CRC Press, 2022, 1160–1165. DOI: 10.1201/9781003348443.

[2] H. C. Bui, D. K. Trinh, and M. T. Nguyen, (2022) *"Effect of web stiffeners on lateral buckling of I-section simply supported beam"* **Steel Construction *15***: 121–130. DOI: 10.1002/stco.202100007.

[3] A. Shaat, A. Matloub, A. Ibrahim, and A. Dessouki, (2022) *"Effect of web stiffeners on the lateral distortional buckling of channel section with hollow flanges"* **Ain Shams Engineering Journal *13***: 101517. DOI: 10.1016/j.asej.2021.06.003.

[4] P. Palanivelu, K. Kaliyamoorthi, A. R. Jabarullah, and R. Samymuthu, (2024) *"Nonlinear Behavior of Cold-Formed Steel Columns: Investigating the Influence of Stiffener on Strength and Buckling Resistance"* **Engineering Proceedings *59***: 148. DOI: 10.3390/engproc2023059148.

[5] O. P. Deepak and P. Aravinth. "Numerical Investigation on Cold-Formed Steel Web Stiffened Lipped Channel Columns Subjected to Local-Distortional Interaction Mode Buckling". In: *International Conference on Advances in Materials Research*. Springer, 2019, 615–628. DOI: 10.1007/978-981-15-8319-3_61.

[6] L. Jiang, J. He, X. Ma, Y. Hu, Z. Chen, Z. Zhang, and H. Yang, (2024) *"Compressive behavior of novel cold-formed steel built-up closed L-shaped section columns"* **Journal of Building Engineering *86***: 108748. DOI: 10.1016/j.jobe.2024.108748.

[7] J. Hua, Z. Yang, F. Wang, X. Xue, N. Wang, and L. Huang, (2022) *"Relation between the metallographic structure and mechanical properties of a bimetallic steel bar after fire"* **Journal of Materials in Civil Engineering *34***: 04022193. DOI: 10.1061/(ASCE)MT.1943-5533.0004351.

[8] W.-J. Dan, R.-B. Gou, M. Yu, Y.-B. Ge, and T.-J. Li, (2022) *"Experimental study on the post-fire mechanical behaviours of structural steels"* **Journal of Constructional Steel Research *199***: 107629. DOI: 10.1016/j.jcsr.2022.107629.

[9] G.-Q. Li, H. Lyu, and C. Zhang, (2017) *"Post-fire mechanical properties of high strength Q690 structural steel"* **Journal of Constructional Steel Research *132***: 108–116. DOI: 10.1016/j.jcsr.2016.12.027.

[10] W. Wang, Y. Li, Z. Wang, and S. Pang, (2024) *"Experimental and numerical study on the behavior of high strength Q960 steel columns after fire exposure"* **Thin-Walled Structures *198***: 111748. DOI: 10.1016/j.tws.2024.111748.

[11] X. Xue, T.-M. Chan, and B. Young. "Numerical investigation on post–fire resistance of cold–formed Q960 ultra high strength steel channel section stub columns". In: *Structures*. ***66***. Elsevier, 2024, 106776. DOI: 10.1016/j.istruc.2024.106776.

[12] X. Lan, S. Li, and O. Zhao, (2021) *"Local buckling of hot-rolled stainless steel channel section stub columns after exposure to fire"* **Journal of Constructional Steel Research *187***: 106950. DOI: 10.1016/j.jcsr.2021.106950.

[13] C. Maraveas, Z. Fasoulakis, and K. D. Tsavdaridis, (2017) *"Post-fire assessment and reinstatement of steel structures"* **Journal of structural fire engineering *8***: 181–201. DOI: 10.1108/JSFE-03-2017-0028.

[14] T. Molkens, K. A. Cashell, and B. Rossi, (2021) *"Post-fire mechanical properties of carbon steel and safety factors for the reinstatement of steel structures"* **Engineering structures *234***: 111975. DOI: 10.1016/j.engstruct.2021.111975.

[15] J.-M. Franssen and V. Kodur. "Residual load bearing capacity of structures exposed to fire". In: 2001, 1–12. DOI: 10.1061/40558(2001)89.

[16] D. Pantousa, T. Karavasilis, and C. Maraveas, (2022) *"Numerical investigation of the post-fire performance of steel columns"* **Buildings *12***: 288. DOI: 10.3390/buildings12030288.

[17] W. Wang and T. Liu, (2016) *"Experimental and numerical study on post-fire behavior of high-strength Q460 steel columns"* **Advances in structural engineering *19***: 1873–1888. DOI: 10.1177/1369433216649390.

[18] J. Yang, X. Zhou, W. Wang, L. Xu, and Y. Shi, (2023) *"Fire resistance of box-shape cold-formed steel built-up columns failing in global buckling: Test, simulation and design"* **Thin-Walled Structures *183***: 110433. DOI: 10.1016/j.tws.2022.110433.

[19] K. Luo, H. Li, J. Yang, S. Fang, F. Yan, J. Yu, X. Han, Y. Xu, and X. Ning, (2025) *"Research on post-fire cold-formed steel back-to-back built-up columns with local buckling"* **Thin-Walled Structures *209***: 112883. DOI: 10.1016/j.tws.2024.112883.

[20] K. Luo, J. Yang, F. Yan, S. Fang, J. Yu, and H. Li, (2025) *"Behavior of the cold-formed steel back-to-back built-up columns with distortional buckling after exposure to high temperatures"* **Fire Technology**: 1–25. DOI: 10.1007/s10694-025-01766-2.

[21] R. Zhang, W. Wang, W. Zeng, and J. Wang. "Local buckling behavior of cold-formed steel box-shaped built-up columns after fire exposure". In: *Structures*. ***84***. Elsevier, 2026, 110952. DOI: 10.1016/j.istruc.2025.110952.

[22] B. Standard, (1993) *"Eurocode 3—Design of steel structures—"* **Bs En *1***: 2005.

[23] K. Roy, B. Chen, Z. Fang, A. Uzzaman, X. Chen, and J. B. P. Lim, (2021) *"Local and distortional buckling behaviour of back-to-back built-up aluminium alloy channel section columns"* **Thin-Walled Structures *163***: 107713. DOI: 10.1016/j.tws.2021.107713.

[24] L. Zhang, F. Wang, Y. Liang, and O. Zhao, (2019) *"Press-braked S690 high strength steel equal-leg angle and plain channel section stub columns: Testing, numerical simulation and design"* **Engineering Structures *201***: 109764. DOI: 10.1016/j.engstruct.2019.109764.

[25] F. Wang, O. Zhao, and B. Young, (2020) *"Testing and numerical modelling of S960 ultra-high strength steel angle and channel section stub columns"* **Engineering Structures *204***: 109902. DOI: 10.1016/j.engstruct.2019.109902.

[26] A. E. Hady, M. E. Aghoury, S. Ibrahim, and E. Amoush, (2022) *"Experimental investigation of steel built-up beam-columns composed of tracks and channels cold-formed sections"* **Journal of Building Engineering *51***: 104295. DOI: 10.1016/j.jobe.2022.104295.